

Behaviors of Selected 2p-valence Impurity Elements in Liquid Lead-Bismuth Eutectic

Junhyoung Gil and Takuji Oda*

Department of Energy Systems Engineering, Seoul National University, 1 Gwanak-ro, Gwanak-gu, Seoul 08826

*Corresponding author: oda@snu.ac.kr

1. Introduction

Liquid lead-bismuth eutectic (LBE), a designated coolant for an LBE-cooled fast reactor (LFR) as well as a target for high power spallation neutron, has good material properties such as low melting point, high boiling point, high heat transfer coefficient, low chemical reactivity with water and air, and high neutron spallation [1]. However, its highly corrosive characteristic for structural steels gives nuclear engineers a critical challenge in terms of material integrity and safety of the LFR.

Impurities in liquid LBE play an important role in increasing or decreasing the corrosion rate. It is widely known that controlling the O concentration is important in that adequate O concentration can mitigate corrosion by forming a protective oxide layer on steels [2–4]. In addition to oxygen, it is also proposed that nitrogen may act as a corrosion inhibitor with even more flexibility and stability to control [5]. Moreover, interstitial impurities in the steel such as oxygen, nitrogen, and carbon affect the dissolution of steel components into LBE [6,7].

Thus, it is of great importance to understand and control the behaviors of these impurities in LBE, which is related to the structural integrity and the comprehensive safety of the LFR. Such fundamental research is expected to provide the knowledge base needed to solve important issues on liquid LBE such as steel corrosion and radionuclide transport. In the present study, we analyzed the behaviors of selected 2p-valence impurity elements – C, N, O, and F – by performing the atomic-scale computational simulations. First-principles molecular dynamics (FPMD) based on density functional theory (DFT) were mainly used.

2. Models and methods

2.1 Simulation Procedure

A cubic supercell consisting of 45 Pb and 56 Bi atoms was prepared as a model LBE system. The system was first equilibrated at 1000 K for 100 ps by classical molecular dynamics (CMD). The LAMMPS code [8] was used here with an embedded-atom method (EAM) potential [9] parameterized by Celino *et al* [10]. Subsequently, FPMD calculations using the VASP code [11] were performed at 1000 K for 15 ps to equilibrate the system. The Perdew-Burke-Ernzerhof (PBE) functional [12] of the generalized gradient approximation (GGA) [13] was utilized to evaluate the exchange-correlation energy. The band energy was sampled over a $2 \times 2 \times 2$ Monkhorst–Pack grid [14], which

has 4 irreducible k-points, with the Methfessel-Paxton smearing scheme of 1st order [15] with a 0.2 eV smearing width.

For the equilibrated LBE system, one impurity atom among C, N, O, and F was introduced at a specific position that is sufficiently distant from the neighboring atoms. Then, another FPMD calculation was performed at 1000 K for 15 ps for each impurity-including LBE system. After the equilibration run of 5 ps, the data of 10 ps was used in the analysis with the following methods.

2.2 Pair correlation function (PCF)

To obtain the structural information on impurity-LBE complexes, a pair correlation function (PCF) was calculated. A PCF represents the number density of the LBE atoms surrounding an impurity atom along the radial distance. The function is expressed as:

$$g_{ij}(r) = \frac{1}{\rho_0 c_i c_j N} \langle \sum_i \sum_{j \neq i} \delta(\vec{r} - \vec{r}_{ij}) \rangle \quad (1)$$

where ρ_0 is the average number density, c_i and c_j are the concentrations of particles i and j , N is the number of particles, and r_{ij} is the distance between the particles i and j . With a given PCF, an average interaction distance and a cutoff radius to first-neighboring atoms (FNAs) were obtained. In addition, a coordination number (CN), which corresponds to the number of FNAs, of an impurity atom was calculated as a volume integral of the PCF:

$$N_{ij} = \int_0^{R_{cutoff}} 4\pi r^2 \rho_0 c_j g_{ij}(r) dr \quad (2)$$

with R_{cutoff} being a cutoff radius to FNAs.

2.3 Projected density of states (pDOS)

To predict the impurity-LBE interaction, the energy levels of atomic orbitals were located by identifying the projected density of states (PDOS). For LBE, 6s and 6p orbitals from each atom interact with each other to form 6s and 6p bands. For 2p orbitals of an impurity, the relative location to the LBE 6s and 6p bands was evaluated. By analyzing the location and the shape of PDOS, it was suggested how an impurity atom interacts with LBE.

Additionally, by evaluating the partial decomposed charge density at specific energy levels determined from pDOS, charge density was visualized to confirm the impurity-LBE interaction expected from PDOS. By constructing and analyzing the isosurface for a decomposed charge density, we visually investigated how an impurity atom interacts with neighboring LBE atoms.

2.4 Static calculations with different FNA compositions

Static calculations were performed with the following procedure to find out the preferences of the impurities either for Pb or for Bi. First, for each impurity case, two configurations (four configurations for the F case) were randomly chosen and optimized. Subsequently, the FNA composition of the impurity atom was changed from all-Bi to all-Pb by replacing the original FNAs with the LBE atoms located far enough from the impurity atom. Finally, the geometry optimization calculation was performed again to locally minimize the potential energy of each system. The preferences were suggested for each impurity by checking the dependence of the system potential energy on the FNA composition.

3. Results and Discussions

3.1. Pair correlation function (PCF)

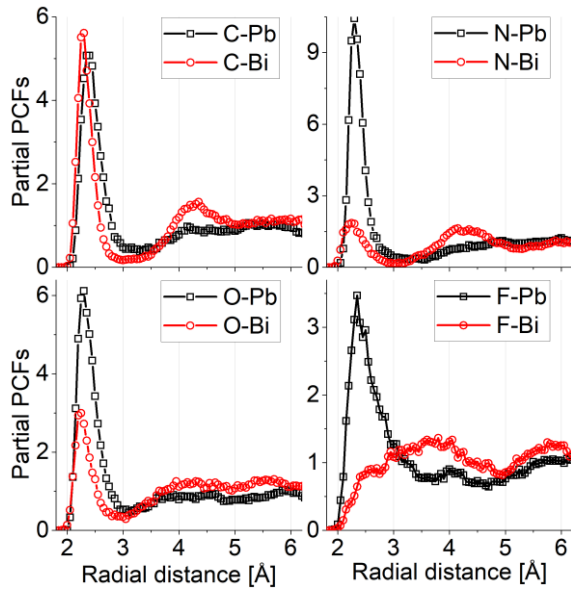


Fig. 1. PCFs for impurity-Pb and impurity-Bi. The x-axis is the radial distance (1.8 Å – 6.2 Å) from the impurity atom.

Table I: Characteristic quantities obtained from the PCFs.

Impurity	C	N	O	F	
Average interaction distance [Å]	2.30	2.30	2.25	2.40	
Cutoff radius to FNAs [Å]	3.20	3.15	3.05	2.75	
CN	Pb	2.3	3.2	2.4	1.5
	Bi	2.1	1.0	1.4	0.5
	Total	4.4	4.2	3.8	2.1

Fig. 1 shows the PCFs for impurity-Pb and impurity-Bi. The average impurity-LBE interaction distance was determined with the first local maximum of the function while the cutoff radius to FNAs was determined with the

first local minimum of the function. For the F case, the cutoff radius was adjusted according to a visualization analysis with geometry-optimized F-LBE structures. The partial (Pb and Bi) and the total CNs were calculated using the determined cutoff radii. These three quantities obtained from the PCFs are listed in Table I.

For C, N, and O, the CNs are around 4, and the separation between first-neighboring and next-neighboring atoms is clear in the PCFs. For the geometry-optimized impurity-LBE complexes, tetrahedron-wise shape is mostly seen for these impurities. From these observations, 2p-6p covalent interaction is predicted as the impurity-LBE interaction scheme. Meanwhile, F has the CN of around 2. This low CN comes from the F-LBE complex structure where the two FNAs are predominantly Pb while Bi appears mainly as the next-neighboring atoms from approximately 2.9 Å away from the F atom. The reason for this unique structure should be related to the points that F-2p orbitals can only accommodate one additional electron to form a closed shell and that F has a higher electronegativity compared to LBE and other impurities.

Moreover, for N, O, and F, the first-neighboring peak for Pb is much higher than that for Bi. As a result, the partial CNs for Pb is greater than the partial CNs for Bi for these three impurities. From these findings, it is suggested that N, O, and F prefer to be surrounded by Pb. This preference will be further confirmed and discussed in the section 3.3.

3.2. Projected density of states (pDOS)

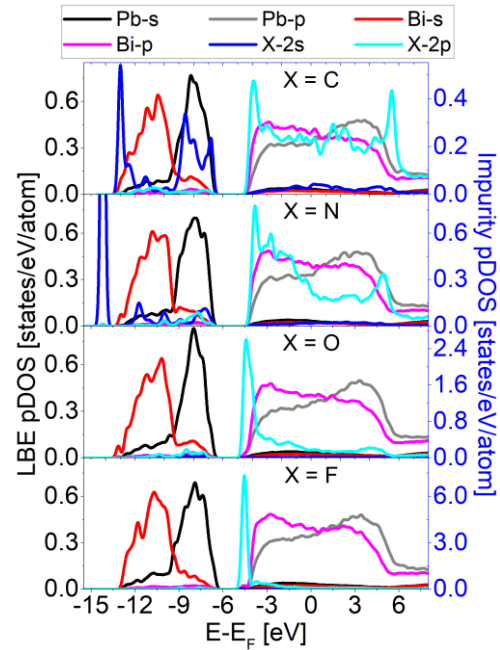


Fig. 2. PDOS evaluated for each impurity-including system. The x-axis is the energy relative to Fermi level (E_F). The left y-axis is scaled for LBE 6s and 6p bands while the right y-axis is scaled for impurity 2s and 2p orbitals.

Table II: Electronegativity (EN) of the impurities and LBE.

Impurity	C	N	O	F	Pb	Bi
EN [eV]	2.55	3.04	3.44	3.98	1.87	2.02
Δ EN [eV]	0.60	1.09	1.49	2.03	0	

Fig. 2 shows the PDOS for each impurity-including system. Among the impurities, the PDOS of C-2p exhibits the most balanced bonding and anti-bonding peaks at around the lower and the upper ends of the LBE-6p band, respectively. This suggests that C interacts with LBE in a covalent manner, which is consistent with the structural analysis results in the previous section.

For 2p-PDOSs in Fig. 2, as the atomic number increases, the bonding orbital peak enlarges, while the anti-bonding peak diminishes. Only the bonding peak is visible for F. This tendency suggests that the impurity-LBE interaction scheme changes from covalent to ionic. Table II compares the electronegativity (EN) [16] of the impurities with Pb and Bi. In general, the interaction between atoms of which EN difference is over 2.0 eV is categorized as ionic. The trend of EN in Table II also indicates a gradual transition of interaction scheme from covalent to ionic.

Fig. 3 shows visualized charge densities for C-LBE and F-LBE complexes. The left figure confirms the covalent interaction between C-2p and LBE-6p. In contrast, almost only the charge density of F-2p is visible in the F case, indicating that the bonding orbitals are dominantly contributed by F-2p orbitals and an electron transfer occurs from LBE atoms to F as ionic interaction.

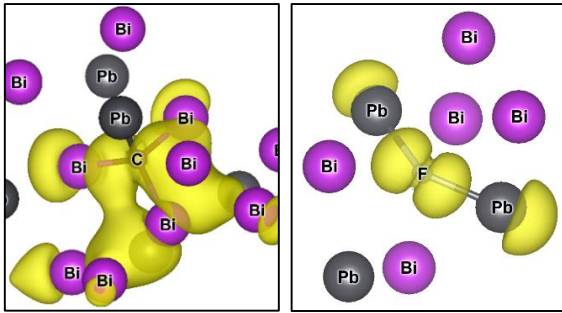


Fig. 3. Visualized charge densities for C-LBE (left) and F-LBE (right) complexes by constructing the isosurface of 0.0008 and 0.003 (electrons/ \AA^3), respectively.

3.3. Static calculations with different FNA compositions

Fig. 4 shows the results for the static calculations with different FNA compositions. Potential energy values for geometry-optimized impurity-including systems were plotted as a function of the Pb fraction in FNAs. Here different “cases” refer to calculation results obtained with different initial configurations, which were randomly selected from the FPMD trajectories.

An increasing trend in the graph means that the potential energy increases as the FNAs changes from Bi to Pb. This can be interpreted that Bi is more favorable for an impurity. A decreasing trend can be interpreted that Pb is more favorable for an impurity. It is seen that generally there is an increasing trend for C and a decreasing trend for N, O, and F. This suggests the preference of C for Bi and the preference of N, O, and F for Pb. This is consistent with the PCF results in the section 3.1 (Fig. 1 and Table I).

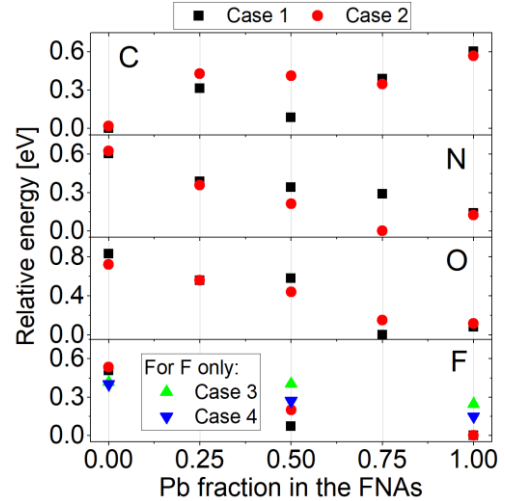


Fig. 4. Potential energy for each impurity-including geometry-optimized system according to the Pb fraction in FNAs. For the x axis, $x=0.00$ means the FNAs are all Bi atoms while $x=1.00$ means the FNAs are all Pb atoms.

4. Conclusion

By performing the FPMD simulations and analyzing the results using several methods, the behaviors of selected 2p-valence impurity elements in liquid LBE were studied. Structural quantities such as impurity-LBE interaction distance and the CNs of the impurities were evaluated using PCFs. The chemical states of the impurities were analyzed by checking PDOS for the impurities and LBE and by visualizing the charge density. The preferences of the impurities were suggested based on the results of the CNs and the static calculations with different FNA compositions.

The CNs of C, N, and O were determined as around 4 with the tetrahedron-wise structure of the impurity-LBE complexes. The CN of F was determined as around 2 with the two FNAs being predominantly Pb. The C-LBE interaction is regarded as the 2p-6p covalent interaction. From C to F, it is predicted from pDOS that the interaction scheme changes from covalent to ionic. Regarding the preferences, C prefers to be surrounded by Bi while N, O, and F prefer to be surrounded by Pb. A more detailed description with additional results and discussions are planned to be presented in the meeting.

REFERENCES

- [1] J. Zhang, Lead-bismuth eutectic (LBE): A coolant candidate for Gen. IV advanced nuclear reactor concepts, *Adv. Eng. Mater.* 16 (2014) 349–356.
- [2] T. Furukawa, G. Müller, G. Schumacher, A. Weisenburger, A. Heinzl, K. Aoto, Effect of oxygen concentration and temperature on compatibility of ODS steel with liquid, stagnant Pb45Bi55, *J. Nucl. Mater.* 335 (2004) 189–193.
- [3] J. Zhang, P. Hosemann, S. Maloy, Models of liquid metal corrosion, *J. Nucl. Mater.* 404 (2010) 82–96.
- [4] N. Li, Active control of oxygen in molten lead-bismuth eutectic systems to prevent steel corrosion and coolant contamination, *J. Nucl. Mater.* 300 (2002) 73–81.
- [5] A. Arkundato, Z. Su'ud, Sudarko, M. Hasan, M. Celino, Molecular dynamics simulation of corrosion mitigation of iron in lead-bismuth eutectic using nitrogen as corrosion inhibitor, *J. Phys. Conf. Ser.* 622 (2015).
- [6] J. Zhang, Corrosion by Liquid Lead and Lead-bismuth: Experimental Result Review and Analysis, 2008.
- [7] E.M. Lyutyi, Problems of high-temperature liquid-metal corrosion of refractory metals and alloys, *Sov. Mater. Sci.* 24 (1989) 441–445.
- [8] S. Plimpton, for Short - Range Molecular Dynamics 1 Introduction, *J. Computat. Phys.* 117 (1995) 1–42.
- [9] M.S. Daw, M.I. Baskes, Embedded-atom method: Derivation and application to impurities, surfaces, and other defects in metals, *Phys. Rev. B.* 29 (1984) 6443–6453.
- [10] M. Celino, R. Conversano, V. Rosato, Atomistic simulation of liquid lead and lead-bismuth eutectic, *J. Nucl. Mater.* 301 (2002) 64–69.
- [11] G. Kresse, J. Hafner, Ab initio molecular dynamics for liquid metals, *Phys. Rev. B.* 47 (1993) 558–561.
- [12] J.P. Perdew, K. Burke, M. Ernzerhof, Generalized gradient approximation made simple, *Phys. Rev. Lett.* 77 (1996) 3865–3868.
- [13] J. Perdew, J. Chevary, S. Vosko, K. Jackson, M. Pederson, D. Singh, C. Fiolhais, Atoms, molecules, solids, and surfaces: Applications of the generalized gradient approximation for exchange and correlation, *Phys. Rev. B.* 46 (1992) 6671–6687.
- [14] H.J. Monkhorst, J.D. Pack, Special points for Brillouin-zone intergrations, *Phys. Rev. B.* 13 (1978) 5897–5899.
- [15] M. Methfessel, A.T. Paxton, High-precision sampling for Brillouin-zone integration in metals, *Phys. Rev. B.* 40 (1989) 3616–3621.
- [16] D.R. Lide, *CRC Handbook of Chemistry and Physics*, 84th ed., CRC Press LLC, Boca Raton, Florida, 2003.

ACKNOWLEDGEMENTS

This research was supported by National Research Foundation (NRF) of Korea under Nuclear Research & Development Program and BK 21 plus project of Seoul National University. The computer simulation was performed using supercomputers and technical support provided by the National Institute of Supercomputing and Network at the Korea Institute of Science and Technology Information (Project-ID: KSC-2017-C2-0034).